Hindawi
Journal of Nanomaterials
Volume 2022, Article ID 2173629, 10 pages
https://doi.org/10.1155/2022/2173629

Research Article

Stress-Induced Structural Phase Transition in Polystyrene/$NaYF_4$: Eu^{3+} Photoluminescent Electrospun Nanofibers

Sanjeev Kumar,[1] **Garima Jain**,[2] **Kuldeep Kumar**,[3] **Ashish Gupta**,[4] **J. S. Tawale**,[5] **B. P. Singh**,[4] **S. R. Dhakate**,[4] **and P. D. Sahare**[6]

[1]*Department of Physics, R. K. (PG) College Shamli, C. C. S. University Meerut, UP-247776, India*
[2]*Department of Physics, D. A. V. (PG) College Muzaffarnagar, C. C. S. University Meerut, UP-251001, India*
[3]*Department of Physics, S.G.T.B. Khalsa College, University of Delhi, Delhi-110007, India*
[4]*Advanced Carbon Products and Metrology Section, Advanced Materials and Devices Metrology Division, CSIR-National Physical Laboratory, Delhi-110012, India*
[5]*Indian Reference Materials, CSIR-National Physical Laboratory, New Delhi-110012, India*
[6]*Department of Physics and Astrophysics, University of Delhi, Delhi-110007, India*

Correspondence should be addressed to Sanjeev Kumar; sanjeev.raonpl@gmail.com

Received 26 November 2021; Accepted 24 March 2022; Published 13 April 2022

Academic Editor: Leander Tapfer

Polystyrene (PS) composite nanofibers were successfully fabricated by embedding $NaYF_4$: Eu^{3+} nanophosphor into the PS matrix via electrospinning. The photoluminescence spectra, surface morphology and crystal structure of nanofibers were characterized by photoluminescence spectroscopy, scanning electron microscopy, and X-ray diffractometer, respectively. Stress-induced α-$NaYF_4$: Eu^{3+} (cubic) to β-$NaYF_4$: Eu^{3+}(hexagonal) structural phase transformation was observed in the nanofibers. The stress-induced phase transformation provides enough space for tailoring the properties of novel nanostructures. The composite nanofibers exhibited blue emission with 239 nm excitation wavelength. The XRD pattern of espun nanofibers confirmed the successful incorporation of 5% $NaYF_4$: Eu^{3+} nanophosphors into the PS matrix. Brilliant values of the chromaticity coordinates of the prepared photoluminescent nanofibers (PLNs) predict their possible use in blue solid-state lighting applications.

1. Introduction

The twenty-first century is enriched by various nanostructures and nanomaterials such as nanotubes, nanofibers, nanoribbons, nanowires, nanocubes, and nanobelts. One-dimensional (1-D) nanofibers have gained significant attention in the research community due to their unique and extraordinary properties among the various nanostructures. Nanofibers have a diameter of less than 100 nm with very high porosity. The high surface area to volume ratio makes them unique for diverse applications such as optoelectronics, biomedical engineering, luminescent fabrics, solar sensors, food packaging, and nanotechnology [1–4]. Among many available techniques, electrospinning is popular in producing long, continuous, fine fibers of variable diameter [5]. In addition to compatible solvent with polymer, some quantity of surface tension solvents or a small amount of pyridine/ionic salts into the solution helps to obtain nanofibers with a small diameter [6].

In recent years, the fabrication of polyacrylonitrile (PAN), polyethylene oxide (PEO), poly (methyl methacrylate) (PMMA), polyvinylidene difluoride (PVdF), poly (vinyl alcohol) (PVA), poly (vinyl pyrrolidone) (PVP), and PS electrospun polymeric light-emitting nanofibers has been studied with different functional additives [7–11]. Herein, polystyrene is considered for the preparation of nonbiodegradable photoluminescent nanofibers using the electrospinning technique. Polystyrene is composed of a long chain of a hydrocarbon having excellent properties such as stiffness, surface quality, and transparency. Therefore,

polystyrene is being utilized in different areas of research. Generally, PS is inert which does not show emission in the visible region [12, 13].

Recently, it can be seen that upconversion nanophosphors (UNCPs) are playing a vital role in biosensing, bioimaging, and solid-state lighting applications. UNCPs are nanoparticles, nanocrystals and microcrystals of lanthanide-doped rare earth fluorides [14, 15]. Several studies have been reported on Eu-doped phosphors with different hosts such as Sr_2InTaO_6, Lu_2O_3, GdOF, $NaYF_4$, and $(TTA)_3$phen for solid state lightening applications [16–22]. Eu^{3+} ions show outstanding luminescent properties among lanthanides. Sodium yttrium fluoride ($NaYF_4$) is a wonderful up or down conversion host lattice. $NaYF_4$ leads to intensify the luminescent properties significantly. $NaYF_4$ nanophosphors show a phase transformation in the structure from α-$NaYF_4$ (cubic) to β-$NaYF_4$ (hexagonal) by changing external parameters like temperature and fabrication process. The lanthanide-doped hexagonal phase of $NaYF_4$ nanocrystals exhibits marvelous luminescence properties because of its low phonon energy [23–26].

Residual stress is one of the important mechanical signatures of atomic and molecular scale in a nonequilibrium state. The stress is generally occurred in the materials by the action of external fields, which is an ambient outcome of solid materials processing at the nanoscale. It remains in the materials even after the removal of applied forces. Usually, as materials are processed for the development of new structures, they are influenced by the nonequilibrium state [27]. The stress performs a significant role in tailoring the performance and reliability of the nanostructures. During the fast fabrication processes, the stress is directly related to the macromolecule chain locking of polymer matrices [28]. The polymeric products demonstrate the stress during the synthesis of thin films, fibers and devices at the nanoscale. Molecular weight, elastic stiffness and glass transition temperature of polymer matrix are the important factors that are contributing to the stress-like phenomena. Therefore, stress is passed on from the polymer matrix to the embedded nanoparticles by the interfacial shear during the synthesis processes [29, 30].

Few research studies have been reported on the photoluminescence properties of PS electrospun nanofibers using inorganic and organic nanoparticles as functional additives. Inorganic nanoparticles incorporating PS composite electrospun nanofibers revealed photoluminescence emission characteristics peaks from 510 to 615 nm, whereas emission peaks were observed from 532 to 612 nm for the organic additive-based PS nanofibers [31–33]. In the present article, facile fabrication of PS composite nanofibers using the electrospinning technique is reported. A phase transformation of $NaYF_4$ from cubic (Fm3m) to hexagonal ($P6_3/mmc$) has been observed for polymeric electrospun nanofibers. PS polymer was used as a novel material for incorporating and aligning the synthesized phosphor material in nanofiber morphology. So, the novelty of the material lies in the novel precursor nanofibers fabricated incorporating the Eu^{3+} doped $NaYF_4$ material and observation of phase change in the synthesized material after incorporation. The study will give insight to the readers about the new electrospinning technique for PLNs fabrication with occurred changes in material via stress induced during electrospinning. The characteristic emission peak is observed at 612 nm, which is possibly efficient for illuminating the solid-state lighting applications.

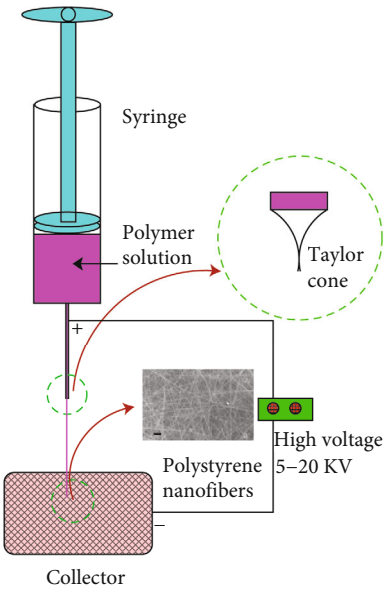

Figure 1: Illustration of the electrospinning process for the preparation of PS composite nanofibers.

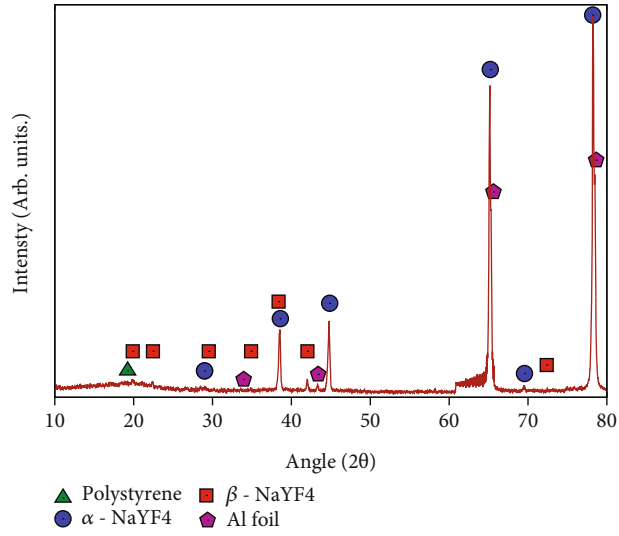

Figure 2: X-ray diffractogram of PS composite nanofibers. PS (green triangle), α-$NaYF_4$: Eu^{3+} (blue circle), β-$NaYF_4$: Eu^{3+} (red square), and Al-foil (violet pentagon) peaks are shown with different asterisks.

2. Materials and Methods

2.1. Materials. All required materials of 99.9% purity were obtained from Thomas Baker Chemicals Pvt. Ltd., Mumbai, India, for the preparation of the nanophoshor. The reagents have been utilized without any purification in the

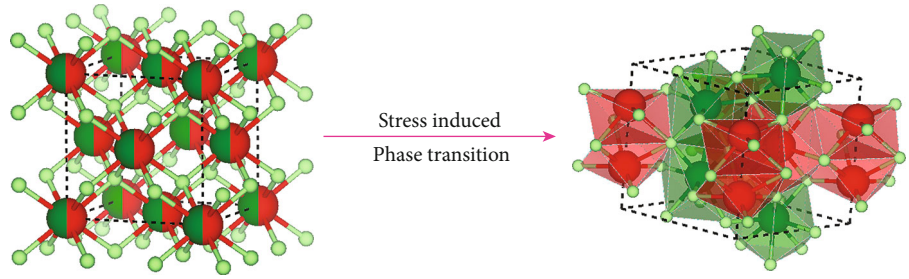

Figure 3: Illustration of the stress-induced phase transition of α-$NaYF_4$ to β-$NaYF_4$ crystal structure (red→ sodium (Na), green→ yttrium (Y), and sea green → fluorine (F)). (a) Crystal structure of α-$NaYF_4$. (b) Crystal structure of β-$NaYF_4$

experimental process. $NaYF_4$: Eu^{3+} nanophosphors were synthesized as similar as our previous study [34].

2.2. Methods: Electrospinning. Nanofibers were fabricated using an electrospinning machine, ESPIN-NANO PICO, Chennai. 25 mg of nanophosphors was added in 4.6 gm of DMF solution. Immediately, ultrasonication of the solution has been done for 45 minutes at 40°C temperature. Furthermore, 500 mg of polystyrene was poured into the same solution and sonicated for 90 minutes. In addition, a 12-hour vigorous magnetic stirring was given to the polymeric solution at room temperature. Uniform dispersed solution of PS and nanophosphors has been obtained from the constant magnetic stirring process. Consequently, a uniform solution was added in a syringe having 24 nozzle gauges of a needle for electrospinning.

Figure 1 shows the schematic design of the electrospinning process for the preparation of PS/$NaYF_4$: Eu^{3+} PLNs. Needle tip to collector distance was kept between 20 cm and 18 kV, and DC voltage was applied between them. The diameter and shape of the nanofibers were controlled by applying high potential. As the potential increases up to the critical limit [35], the flow rate of the solution and the speed of the collector were kept at 0.3 ml/h and 2000 rpm, respectively. Espun nanofibers were collected on aluminum sheets of size 14 cm ×13 cm having 0.158 mm thickness.

3. Results and Discussion

3.1. X-Ray Diffraction. X-ray diffraction pattern of PS composite nanofibers was taken by Rigaku Japan X-ray diffractometer having Cu-K_α radiation with a wavelength of $\lambda = 0.15406$ nm in the 2θ range of 10-80°. Figure 2 demonstrates the X-ray diffractions of PS composite nanofibers. The peak centered at $2\theta = 19°$ (green triangle) is assigned for PS. The aluminum (Al) foil peaks are 38.57°, 44.75°, 65.32°, and 78.48° (violet pentagon). The blue circled peaks 28.22°, 42.02°, 58.22°, 69.53°, and 78.25° (blue circle) correspond to α-$NaYF_4$ (Cubic, JCPDS No. 77-2042) (Fm3m) are associated to crystal planes (111), (220), (222), (400), and (420), respectively. While the red squared peaks at 19.88°, 29.03°, 34.88°, 38.46°, 43.31°, and 72.44°(red square) corresponding to β-$NaYF_4$ (hexagonal, JCPDS No. 28-1192, $P6_3/mmc$) are associated to crystal planes (111), (110), (200), (111), (201) and (311), respectively.

Table 1: A comparative of the refractive index of PVA, PMMA, PAN, and PS.

Polymer	Refractive index
PVA	1.477@632 nm [43]
PMMA	1.483@ 632 nm [44]
PAN	1.52@600 nm [45]
PS	1.586@632 nm [46]

When the α-$NaYF_4$ parent cubic phase is subjected to external stress, it shows the transition into the β-$NaYF_4$ daughter hexagonal phase, which has lower energy than the parent phase. The cubic and hexagonal phases are present in the PS/$NaYF_4$: Eu^{3+} nanofibers. This phase transition occurs because of the stress being transferred from the PS polymer to the embedded unit cells of nanophosphors within the fibers. The diffraction peaks of α-$NaYF_4$: Eu^{3+} are attributed to pure cubic $NaYF_4$, whereas XRD peaks of β- $NaYF_4$: Eu^{3+} are assigned to hexagonal $NaYF_4$ (Figure 2). When Eu^{3+} ions are dispersed with such disordered crystal, the coordination environment of Y^{3+}, around the ions will deform the lattice. It happens due to the mismatch of ionic radius of Y^{3+} (0.89 A°) and Eu^{3+} (0.95 A°). A left shift of the X-ray peak juxtaposed with the peak of a single crystal reveals a decrease in d-spacing. It means the tensile stress acting on the crystal structure and vice versa an increase in d-spacing is the signature of compressive stress. Then, the stress is calculated by the multiplication of the average strain and elastic constant of the nanofiber. As strain is fundamental, in this study, PS composite nanofiber concerning strain is characterized [36–38].

Figure 3 indicates the phase transition in the $NaYF_4$ crystal structure. The visualization for electronic and structure analysis (VESTA) tool has been used to visualize the structure [39]. The applied tensile stress minimizes the energy barrier for α to β phase transition, while it maximizes the energy barrier for the reverse transition from the β phase back to the α phase may occur. Shear deformation is the principal operation of the slip system. The effective stress can be large enough to overcome the energy barrier or

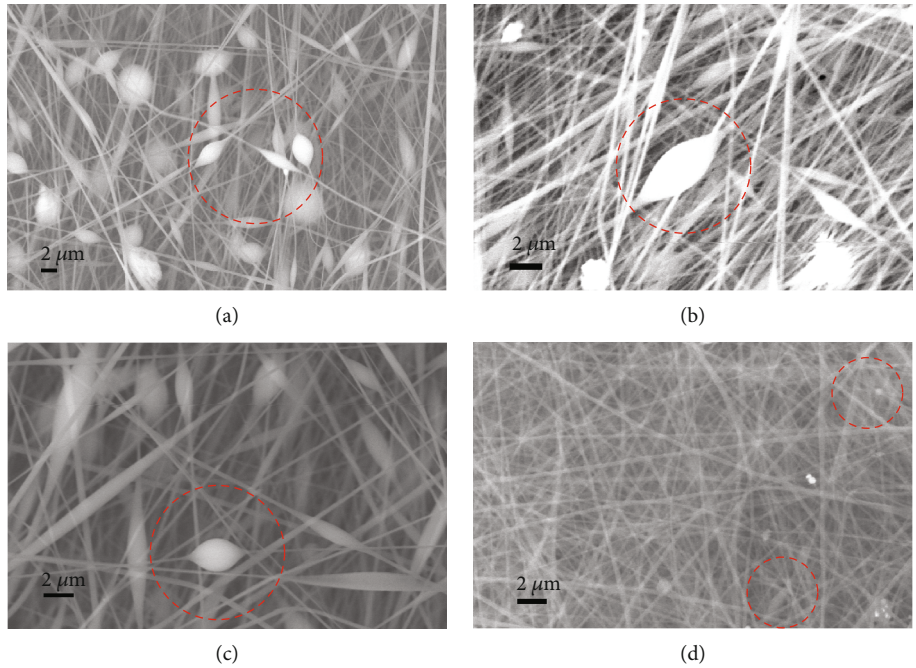

FIGURE 4: The SEM pictures of PS composite nanofibers at 5% with different flow rates (a) 0.1 ml/h, (b) 0.15 ml/h, (c) 0.2 ml/h and (d) 0.3 ml/h.

Burger's vector and exceeds the critical shear stress required to activate the lattice plane slide/slip [40, 41].

Typically, polymer structures consist of both amorphous and crystalline linear molecular chains. The properties of the polymer matrices are depended upon the arrangement of the molecules in structure. The polymeric structure is said to be crystalline if the alignment of the linear molecules is systematic, whereas the unsystematic arrangement of the molecules approaches to amorphous structures. The crystalline polymers can be understood by the well-known folded chain theory for polymeric structures. The beauty of crystalline polymer matrices is that they are brittle in nature which leads them to better optical properties. It is also to be noted here that higher crystalline polymer matrices have a high refractive index, which makes them translucent in nature, while the amorphous polymer matrices show their transparent nature entirely [42]. Table 1 shows the refractive indices of a few polymer matrices. Crystalline polymer matrices are that they are brittle in nature which leads them to better optical properties. Table 1 shows the refractive indices of a few polymer matrices.

Kumar et al. have incorporated the $NaYF_4$: Eu^{3+} nanophosphors into the PVA [34], PAN [47], and PMMA [48] matrices using electrospinning. However, stress-induced phase transition didn't find in electrospun nanofibers with the phosphor nanoparticles Zare et al. observed that the stress is transferred from the polymer matrix to embedded nanoparticles in a polymeric nanocomposite. An imperfect interface like a polymer cannot bear the large interfacial shear stress. Such deformation minimizes the interfacial shear stress that initiates a slower transfer of normal stress in platelets/nanoparticles [49–51]. When a polymer is crystalline enough, it transfers the maximum stress to the embedded nanoparticles resulting in the stress-induced phase transition which is observed in polymeric nanocomposites and nanofibers. The PS polymer is more crystalline than PVA, PMMA and PAN matrices, which enables PS to transfer the shear stress to the nanophosphor. The hexagonal phase of β-$NaYF_4$ UNCPs is more stable than α-$NaYF_4$ which has been observed in PS/$NaYF_4$: Eu^{3+} PLNs via phase transformation. The PS nanofibers get stressed during the electrospinning process. Hence, they transferred the stress to the cubic unit cell, resulting in the hexagonal phase of the nanophosphor being obtained. The strain is calculated for (111) and (222) planes 0.000521 and 0.002741, respectively. This amount of strain is enough to activate the slip/slide (111) plane of α-$NaYF_4$ to the basal slip plane (0001) of the β-$NaYF_4$ phase.

The cubic structure of $NaYF_4$ has been confirmed by XRD with the lattice parameters (cal) of $a = b = c = 5.48A^{\circ}$ along with the angles $\alpha = \beta = \gamma = 90^{o}$, whereas the hexagonal structure affirmed with the lattice parameters of $a = b = 5.96A^{\circ}$, $c = 3.53A^{\circ}$, $\alpha = \beta = 90^{o}$ and $\gamma = 120^{o}$. The crystal size of α and β crystals has a diameter of 46.18 nm and 70.25 nm in PS nanofiber, respectively. [52]

3.2. Surface Morphology. ZEISS EVO 18 scanning electron microscopy (SEM) has been used to investigate the morphology of the electrospun nanofibers. Figures 4(a)–4(d) show the SEM micrographs of randomly aligned PS/NaYF4: Eu^{3+} nanofibers with different flow rates 0.1, 0.15, 0.2 and 0.3 ml/h, respectively, at 5%. The flow rates 0.1, 0.15, 0.2 and 0.3 ml/h are optimized during the electrospinning process and found that 0.3 ml/h flow rate is appropriate for the good surface morphology of espun nanofibers. Not only the concentration but the flow rate of PS solution has also

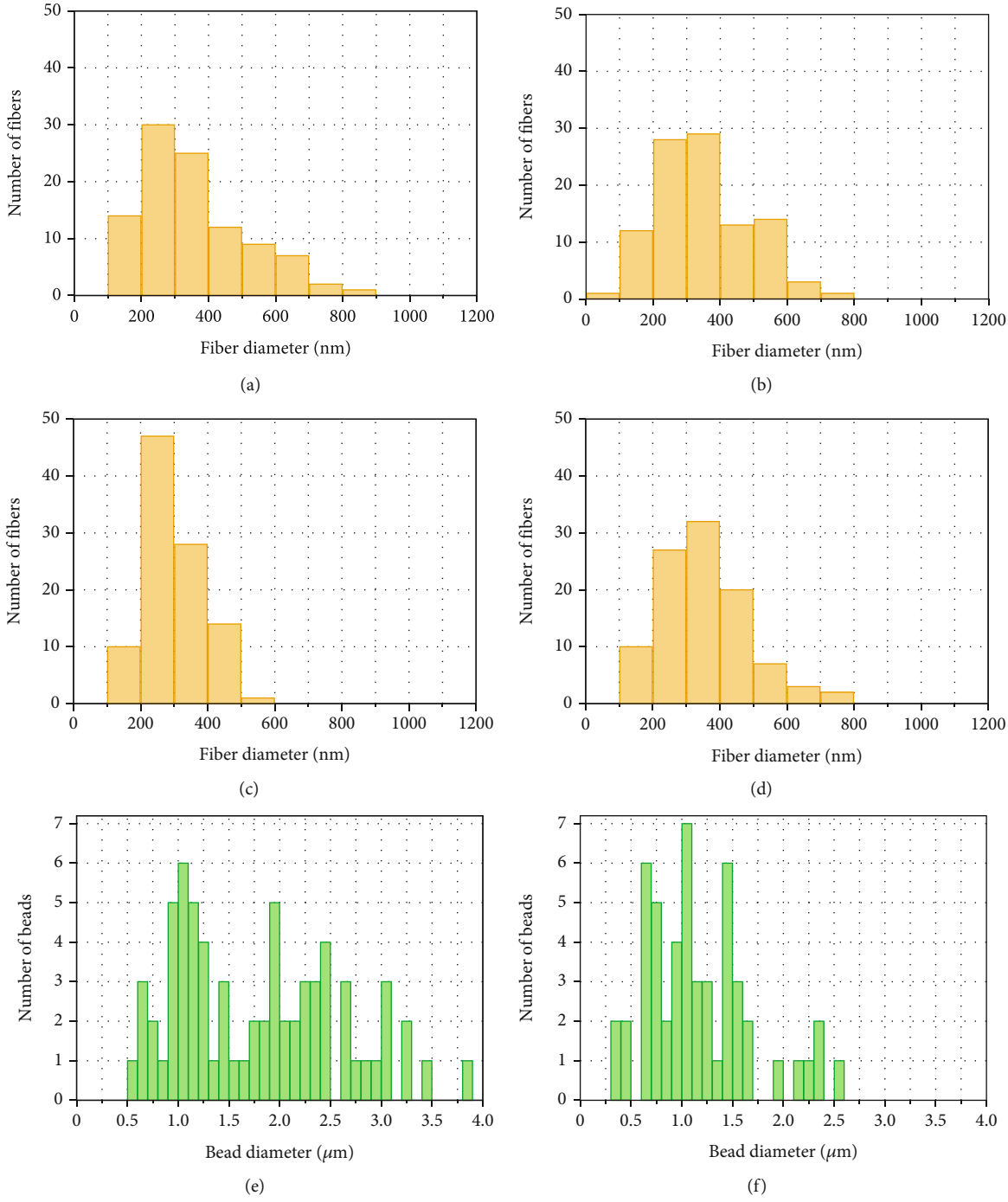

Figure 5: Continued.

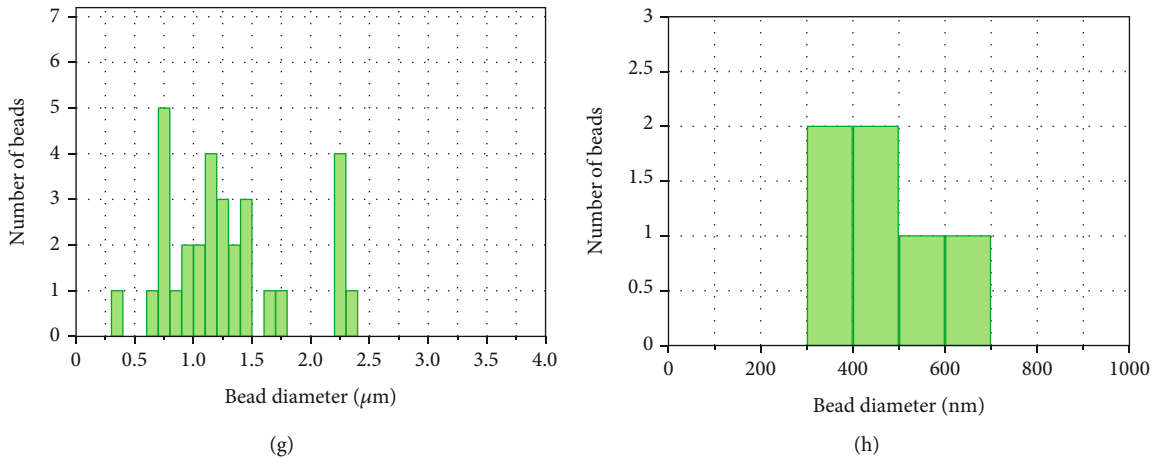

Figure 5: Texture analysis of PS nanofibers: (a–d) show the fiber diameter distribution (FDD) at 0.1, 0.15, 0.2 and 0.3 ml/h flow rate and (e–h) show the bead size distribution (BSD) @ 0.1, 0.15, 0.2, and 0.3 ml/h flow rate.

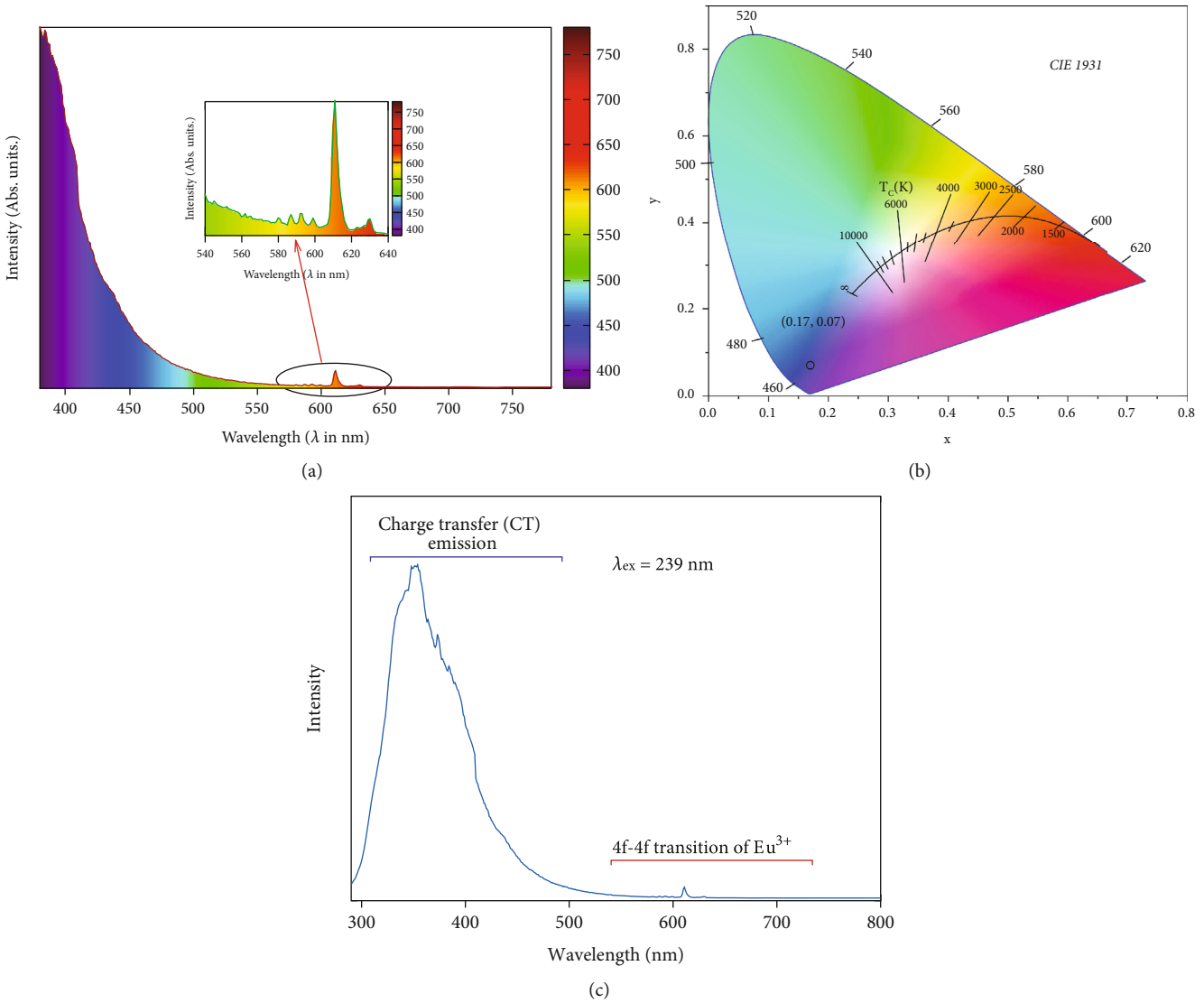

Figure 6: (a) Photoluminescence (PL) spectra of PS composite nanofibers at 5%, (b) chromaticity (CIE-1931) emission coordinates ($X = 0.17$, $Y = 0.07$) extracted from the PL spectra of nanofibers corresponding to 239 nm excitation wavelength, and (c) charge transfer (CT) band in comparison with f-f transitions bands.

Table 2: Experimental Judd-Ofelt intensity parameters, radiative emission rates (Arad), nonradiative decay rates (Anrad), intensity ratio, parameter sum efficiency of PS/$NaYF_4$: Eu^{3+} nanofibers.

Complex	Judd-Ofelt intensity parameters ($X\ 10^{-20} cm^2$)		Radiative emission rates (A_{rad}) (s^{-1})	Nonradiative decay rates (A_{nrad}) (s^{-1})	Intensity ratio (I_2/I_1)	Quantum efficiency η (%)
	Ω_2	Ω_4				
PS/$NaYF_4$: Eu^{3+}	5.05	0.40	230.58	7521.35	2.92	2.97

influenced the morphology of electrospun nanofibers. SEM pictures reveal that beads are present in the nanofibers which are prepared by following the flow rates 0.1, 0.15 and 0.2 ml/h. As the flow rates of the PS solution are increased from 0.1 to 0.3 ml/h, the nanofibers become uniform, and their beads almost vanished. Therefore, the flow rate plays a vital role in the electrospinning process. Generally, an accurate flow rate improves the surface morphology of electrospun nanofibers.

The texture analysis of PS composite nanofibers is shown in Figure 5. The diameter of nanofibers and their bead component analysis is shown in the histogram studied by ImageJ software. The average diameter of nanofibers is found 354 nm, 351 nm, 297 nm and 361 nm at 0.1, 0.15, 0.2 and 0.3 ml/h flow rate, respectively, whereas the bead components have the diameter as 1.8 mm, 1.16 mm, 1.,10 mm and 451 nm for the same flow rates.

It is concluded from the histogram from e to h that the number of bead components decreases as the flow rate increases. The obtained nanofiber mat consists of the network-like structure at 5% concentration of nanophosphor in the PS matrix at 0.3 ml/h flow rate with an average diameter of 350 nm.

3.3. Photoluminescence (PL) Spectra. The PL spectra of PS were recorded at 239 nm excitation wavelength using the spectrometer Perkin-Elmer LS 55. The photoluminescence spectra of PS composite beaded nanofibers are shown in Figure 6(a) with an emission peak in the inset. PS composite nanofibers exhibit emission intense peaks at around 590 nm and 612 nm with 239 nm excitation wavelength. The characteristic emission lines shown in the inset are associated with the Eu^{3+} transitions from the excited $^5D_0 \rightarrow {}^7F_J$ level, a transition of Eu^{3+}, where J ranges from 0 to 2, that is, 590 nm, $^5D_0 \rightarrow {}^7F_1$; 612 nm, $^5D_0 \rightarrow {}^7F_2$. The International Commission on Illumination (CIE) 1931 has been utilized to understand the color quality from composite nanofibers.

The color space chromaticity diagram of PS composite nanofibers is shown in Figure 6(b) at 239 nm with the color coordinates of $X = 0.17$ and $Y = 0.07$. The luminescence of Eu^{3+} ions attributes to the phenomenon of excitation which is due to charge transfer (CT), enhancing the emission effectiveness. Figure 6(c) shows that a charge transfer (CT) band is significantly wider and much more intensive in comparison with f-f transitions bands. The nonradiative recombination of the excitons can be controlled through the charge or energy transfer process during the fluorescence quenching. Therefore, $NaYF_4$ emission will not be affected or slightly changed, and hence, the tunability can be achieved.

The Judd-Ofelt intensity parameters were determined using LUMPAC package [53, 54]. All the calculated quantities (Ω_2,Ω_4,A_{rad}, A_{nrad}, I_2/I_1, and η) are shown in Table 2.

4. Conclusions

In conclusion, PS composite nanofibers are fabricated using an electrospinning technique having an average diameter of 361 nm. The morphology of PLNs reveals that an optimum flow rate is required for the preparation of uniform electrospun nanofibers. The bead components lost their identity properly with varying flow rates from 0.1 to 0.3 ml/h. XRD results not only confirmed the phase transition from cubic to hexagonal but also a homogeneous dispersion of $NaYF_4$: Eu^{3+} nanophosphors into the PS matrix. The hexagonal phase is achieved due to the shear stress exerted on the nanofiber. The typical emission transition $^5D_0 \rightarrow {}^7F_2$ exhibits the chemical environment of Eu^{3+} ions. These results demonstrate the possible use of PS espun composite nanofibers in solid-state lighting, biosensing and bioimaging applications. The concentration of the nanophosphors into the PS matrix is also an important factor for affecting the PL properties during electrospinning. By varying the concentration of the nanophosphors in the PS matrix, the PL properties of espun nanofibers can be enhanced in future studies. Future studies will focus on the potential use of PS espun nanofibers in flexible lightening applications.

Data Availability

The data used to support the findings of this study are included within the article. Should further data or information be required, these are available from the corresponding author upon request.

Conflicts of Interest

The authors declare that there are no conflicts of interest regarding the publication of this paper.

Acknowledgments

The authors greatly acknowledged Mr. N. K. Upadhyay for XRD and Dr. Govind Gupta for PL characterization from CSIR-NPL, New Delhi. Moreover, we are grateful to Dr. Y. K. Gautam and Professor B. P. Singh (head) from the Department of Physics, CCSU, Meerut, UP, for SEM characterization. We would like to acknowledge Professor P. Arun from the Department of Electronics, S. G. T. B. Khalsa College, University of Delhi, Delhi, for his continuous support and encouragement.

References

[1] S. Peng, L. Li, Y. Hu et al., "Fabrication of spinel one-dimensional architectures by single-spinneret electrospinning for energy storage applications," *ACS Nano*, vol. 9, no. 2, pp. 1945–1954, 2015.

[2] E. Yang, Z. Xu, L. K. Chur et al., "Nanofibrous smart fabrics from twisted yarns of electrospun piezopolymer," *ACS Applied Materials & Interfaces*, vol. 9, no. 28, pp. 24220–24229, 2017.

[3] J. Lin, B. Ding, J. Yu, and Y. Hsieh, "Direct fabrication of highly nanoporous polystyrene fibers via electrospinning," *ACS Applied Materials & Interfaces*, vol. 2, no. 2, pp. 521–528, 2010.

[4] V. K. Tulasidas, S. L. Belagali, P. Arun, and K. Kumar, "Photoluminescence and applications of Ni: ZnS in photovoltaic cells," *Japanese Journal of Applied Physics*, vol. 57, no. 5, article 052302, 2018.

[5] S. Tang, C. Shao, Y. Liu, and R. Mu, "Electrospun nanofibers of poly(acrylonitrile)/Eu^{3+} and their photoluminescence properties," *Journal of Physics and Chemistry of Solids*, vol. 71, no. 3, pp. 273–278, 2010.

[6] H. Fong, I. Chun, and D. H. Reneker, "Beaded nanofibers formed during electrospinning," *Polymer*, vol. 40, no. 16, pp. 4585–4592, 1999.

[7] Z. Yu, L. Shen, D. Li, E. Y. B. Pun, X. Zhao, and H. Lin, "Fluctuation of photon-releasing with ligand coordination in polyacrylonitrile-based electrospun nanofibers," *Scientific Reports*, vol. 10, no. 1, p. 926, 2020.

[8] M. A. Sobhan, A. Lebedev, L. L. Chng, and F. Anariba, "Rapid fabrication of photoluminescent electrospun nanofibers without the need of chemical polymeric backbone modifications," *Journal of Nanomaterials*, vol. 2018, 7 pages, 2018.

[9] S. G. Itankar, M. P. Dandekar, S. B. Kondawar, and B. M. Bahirwar, "Eu^{3+}-doped polystyrene and polyvinylidene fluoride nanofibers made by electrospinning for photoluminescent fabric designing," *Luminescence*, vol. 32, no. 8, pp. 1535–1540, 2017.

[10] B. Ortac, F. Kayaci, H. A. Vural, A. E. Deniz, and T. Uyar, "Photoluminescent electrospun polymeric nanofibers incorporating germanium nanocrystals," *Reactive & Functional Polymers*, vol. 73, no. 9, pp. 1262–1267, 2013.

[11] A. B. Suryamas, M. M. Munir, T. Ogi, C. J. H. Jr, and K. Okuyama, "Photoluminescent ZrO_2: Eu^{3+} nanofibers prepared via electrospinning," *Japanese Journal of Applied Physics*, vol. 49, no. 11, article 115003, 2010.

[12] B. T. Ho, T. K. Roberts, and L. Steven, "An overview on biodegradation of polystyrene and modified polystyrene: the microbial approach," *Critical Reviews in Biotechnology*, vol. 38, no. 2, pp. 308–320, 2018.

[13] B. G. Kwon, K. Saido, K. Koizumi et al., "Regional distribution of styrene analogues generated from polystyrene degradation along the coastlines of the North-East Pacific Ocean and Hawaii," *Environmental Pollution*, vol. 188, pp. 45–49, 2014.

[14] Q. Yao, P. Hu, P. Sun et al., "YAG: Ce^{3+} transparent ceramic phosphors brighten the next-generation laser-driven lighting," *Advanced Materials*, vol. 32, no. 19, p. 1907888, 2020.

[15] S. Biasco, A. Ciavatti, L. Li et al., "Highly efficient surface-emitting semiconductor lasers exploiting quasi-crystalline distributed feedback photonic patterns," *Light: Science & Applications*, vol. 9, no. 1, pp. 1–11, 2020.

[16] J. Zhao, H. Gao, H. Xu et al., "Structure and photoluminescence of Eu^{3+} doped Sr_2InTaO_6 red phosphor with high color purity," *RSC Advances*, vol. 11, no. 14, pp. 8282–8289, 2021.

[17] N. Dhananjaya, S. R. Yashodha, and C. Shivakumara, "The orange red luminescence and conductivity response of Eu^{3+} doped GdOF phosphor: synthesis, characterization and their Judd-Ofelt analysis," *Materials Research Express*, vol. 6, no. 12, 2019.

[18] A. K. Gangwar, A. Gupta, G. Kedawat et al., "Highly luminescent dual mode polymeric nanofiber-based flexible mat for white security paper and encrypted nanotaggant applications," *Chemistry-A European Journal*, vol. 24, no. 38, pp. 9477–9484, 2018.

[19] Z. Hao, C. Jindeng, and G. Hai, "Electrospinning synthesis and luminescent properties of Lu_2O_3: Eu^{3+} nanofibers," *Journal of Rare Earths*, vol. 28, pp. 232–235, 2010.

[20] C. Li, C. Zhang, Z. Hou et al., "Highly uniform and monodisperse β-$NaYF_4$: Ln^{3+} (Ln = Eu, Tb, Yb/Er, and Yb/Tm) hexagonal microprism crystals: hydrothermal synthesis and luminescent properties," *Inorganic Chemistry*, vol. 46, no. 16, pp. 6329–6337, 2007.

[21] K. W. Krämer, D. Biner, G. Frei, H. U. Güdel, M. P. Hehlen, and S. R. Lüthi, "Hexagonal sodium yttrium fluoride based green and blue emitting upconversion phosphors," *Chemistry of Materials*, vol. 16, no. 7, pp. 1244–1251, 2004.

[22] X. Zhang, S. Wen, S. Hu, L. Zhang, and L. Liu, "Electrospinning preparation and luminescenceproperties of Eu $(TTA)_3$-phen/polystyrene composite nanofibers," *Journal of Rare Earths*, vol. 28, no. 3, pp. 333–339, 2010.

[23] G. Adachi and N. Imanaka, "The binary rare earth oxides," *Chemical Reviews*, vol. 98, no. 4, pp. 1479–1514, 1998.

[24] O. A. Graeve, S. Varma, G. George, D. Brown, and E. Lopez, "Synthesis and characterization of luminescent yttrium oxide doped with Tm and Yb," *Journal of the American Chemical Society*, vol. 89, no. 3, pp. 926–931, 2006.

[25] S. Saha, R. G. S. Pala, and S. Sivakumar, "Catalyzing "cubic-to-hexagonal phase transition in $NaYF_4$ via ligand enhanced surface ordering"," *Crystal Growth & Design*, vol. 18, no. 9, pp. 5080–5088, 2018.

[26] J. Huang, X. Wang, A. Shao, G. Du, and N. Chen, "Growth of β-$NaYF_4$: Eu^{3+} crystals by the solvothermal method with the aid of oleic acid and their photoluminescence properties," *Materials*, vol. 12, no. 22, p. 3711, 2019.

[27] J. Y. Chung, T. Q. Chastek, M. J. Fasolka, H. W. Ro, and C. M. Stafford, "Quantifying residual stressin nanoscale thin polymer films via surface wrinkling," *ACS Nano*, vol. 3, no. 4, pp. 844–852, 2009.

[28] L. F. Francis, A. V. McCormick, D. M. Vaessen, and J. A. Payne, "Development and measurement of stress in polymer coatings," *Journal of Materials Science*, vol. 37, no. 22, pp. 4717–4731, 2002.

[29] C. Androulidakis, D. Sourlantzis, E. N. Koukaras, A. C. Manikas, and C. Galiotis, "Stress-transfer from polymer substrates to monolayer and few-layer graphenes," *Nanoscale Advances*, vol. 1, no. 12, pp. 4972–4980, 2019.

[30] F. Zhang and Y. Liu, *Carbon nanotube fibers and yarns: production, properties and applications in smart textiles*, Elsevier, Amsterdam, 1st edition, 2020.

[31] M. P. Dandekar, S. B. Kondawar, S. G. Itankar, and D. V. Nandanwar, "Luminescence properties of electrospun nanofibers of europium complex Eu (TTA) 3phen/polymers," *Procedia Materials Science*, vol. 10, pp. 580–587, 2015.

[32] Y. Wang, B. Li, Y. Liu et al., "Highly sensitive oxygen sensors based on Cu(i) complex-polystyrene composite nanofibrous membranes prepared by electrospinning," *Chemical Communications*, vol. 39, pp. 5868–5870, 2009.

[33] M. P. Dandekar, S. B. Kondawar, S. G. Itankar, D. V. Nandanwar, and P. Koinkar, "Photoluminescent electrospun europium complex Eu $(TTA)_3$phen embedded polymer blends nanofibers," *Optical Materials*, vol. 85, pp. 483–490, 2018.

[34] S. Kumar, G. Jain, B. P. Singh, and S. R. Dhakate, "Tunable photoluminescence of polyvinyl alcohol electrospun nanofibers by doping of $NaYF_4$: Eu^{3+} nanophosphor," *Journal of Nanomaterials*, vol. 2020, 8 pages, 2020.

[35] A. L. Yarin, S. Koombhongse, and D. H. Reneker, "Taylor cone and jetting from liquid droplets in electrospinning of nanofibers," *Journal of Applied Physics*, vol. 90, no. 9, pp. 4836–4846, 2001.

[36] K. Kumar, P. Arun, C. R. Kant, N. C. Mehra, and V. Mathew, "The effect of cesium metal clusters on the optical properties of cesium iodide thin films," *Applied Physics A: Materials Science & Processing*, vol. 99, no. 1, pp. 305–310, 2010.

[37] K. Kumar, P. Arun, C. R. Kant, N. C. Mehra, L. Makinistian, and E. A. Albanesi, "Effect of residual stress on the optical properties of CsCl thin films," *Journal of Physics and Chemistry of Solids*, vol. 71, no. 3, pp. 163–169, 2010.

[38] K. Kumar, P. Arun, C. R. Kant, and B. K. Juluri, "Metal cluster's effect on the optical propertiesof cesium bromide thin films," *Applied Physics Letters*, vol. 100, no. 24, article 243106, 2012.

[39] K. Momma and F. Izumi, "VESTA 3 for three-dimensional visualization of crystal, volumetric and morphology data," vol. 44, pp. 1272–1276, 2011.

[40] Y. C. Wu, N. J. Ho, and H. Y. Lu, "Dissociation of basal dislocations in hexagonal barium titanate," *Journal of Microscopy*, vol. 220, no. 3, pp. 205–220, 2005.

[41] W. S. Cho, "Structural evolution and characterization of $BaTiO_3$ nanoparticles synthesized frompolymeric precursor," *Journal of Physics and Chemistry of Solids*, vol. 59, no. 5, pp. 659–666, 1998.

[42] M. Wasim, A. Sabir, M. Shafiq, and T. Jamil, *Nanoscale Materials in Water Purification, Chapter 11-Electrospinning: a fiber fabrication technique for water purification*, Elsevier, Amsterdam, 2019.

[43] M. J. Schnepf, M. Mayer, C. Kuttner et al., "Nanorattles with tailored electric field enhancement," *Nanoscale*, vol. 9, no. 27, pp. 9376–9385, 2017.

[44] G. Beadie, M. Brindza, R. A. Flynn, A. Rosenberg, and J. S. Shirk, "Refractive index measurements of poly (methyl methacrylate) (PMMA) from 0.4-1.6μm," *Applied Optics*, vol. 54, no. 31, pp. F139–F143, 2015.

[45] B. Cocilovo, A. Amooali, A. Lopez-Santiago et al., "Effect of modular diffraction gratings on absorption in P3HT: PCBM layers," *Applied Optics*, vol. 52, no. 5, pp. 1025–1034, 2013.

[46] W. M. Haynes, *CRC Handbook of Chemistry and Physics*, CRC Press, 92nd edition, 2011.

[47] S. Kumar, G. Jain, K. Kumar, A. Gupta, B. P. Singh, and S. R. Dhakate, "A novel fabrication of electrospun polyacrylonitrile/$NaYF_4$: Eu^{3+} light emitting nanofibers," *RSC Advances*, vol. 10, no. 42, pp. 24855–24861, 2020.

[48] S. Kumar, G. Jain, K. Kumar, A. Gupta, B. P. Singh, and S. R. Dhakate, "A facile fabrication of poly (methyl methacrylate)/ α-$NaYF_4$: Eu^{3+} tunable electrospun photoluminescent nanofibers," *Applied Nanoscience*, vol. 10, no. 10, pp. 3857–3864, 2020.

[49] Y. Zare, M. Fasihi, and K. Y. Rhee, "Efficiency of stress transfer between polymer matrix andnanoplatelets in clay/polymer nanocomposites," *Applied Clay Science*, vol. 143, pp. 265–272, 2017.

[50] Y. Zare, "New models for yield strength of polymer/clay nanocomposites," *Composites: Part B*, vol. 73, pp. 111–117, 2015.

[51] Y. Zare, "Study on interfacial properties in polymer blend ternary nanocomposites: role of nanofiller content," *Computational Materials Science*, vol. 111, pp. 334–338, 2016.

[52] B. D. Cullity, *Elements of X-Ray Diffraction*, Addison Wesley, New York, 1956.

[53] J. D. L. Dutra, T. D. Bispo, and R. O. Freire, "LUMPAC lanthanide luminescence software: efficient and user friendly," *Journal of Computational Chemistry*, vol. 35, no. 10, pp. 772–775, 2014.

[54] S. R. Yashodha, N. Dhananjaya, S. R. Manohara, and H. S. Yogananda, "Investigation of photoluminescence and dielectric properties of europium-doped LaOCl nanophosphor and its Judd–Ofelt analysis," *Journal of Materials Science: Materials in Electronics*, vol. 32, no. 9, pp. 11511–11523, 2021.